

Fault-Tolerant Control of Electric Ground Vehicles Using a Triple-Step Nonlinear Approach

Yulei Wang , Shuyou Yu, Jingxin Yuan , and Hong Chen , *Senior Member, IEEE*

Abstract—This paper investigates a triple-step approach-based fault-tolerant control (FTC) strategy for in-wheel motor electric ground vehicles, whose purpose is to preserve stability, improve handling with in-wheel motors and/or steering system faults. The proposed scheme is divided into two levels. The first level is the integrated vehicle motion control with model uncertainties, disturbances and the possible actuator faults, in which a triple-step nonlinear controller with on-line updating laws is designed. The second level is the driving reference signal generation, where the triple-step feedback law is used to provide a quantitative driving guidance and a residual signal with threshold for monitoring and evaluating drivers. The proposed FTC scheme not only achieves the vehicle safety but also the high-availability of the closed-loop driver-vehicle system. Simulation results show the effectiveness of the proposed scheme.

Index Terms—Adaptive control, driver-in-the-loop, electric ground vehicles, fault-tolerant control, triple-step control.

NOMENCLATURE

C_a	Aerodynamic drag coefficient.
C_f	Front cornering stiffness.
C_r	Rear cornering stiffness.
F_x	Longitudinal force acting on vehicle center of gravity.
F_{xi}	Longitudinal tire force of the i th wheel.
F_{yi}	Lateral tire force of the i th wheel.
F_{yf}	Front lateral tire force.
F_{yr}	Rear lateral tire force.
M	Mass of the vehicle.
I	Wheel rotational inertia.
I_z	Yaw inertia of the vehicle.

Manuscript received October 31, 2016; revised March 7, 2017, June 28, 2017, November 6, 2017, and February 4, 2018; accepted May 6, 2018. Date of publication May 16, 2018; date of current version August 14, 2018. Recommended by Technical Editor J. Wang. This work was supported in part by the National Nature Science Foundation of China under Grant 61603147, Grant 61573165, Grant 61790561, and Grant 61790564, in part by the Department of Science and Technology of Jilin Province under Grant 20160520107JH, and in part by the Program for China Postdoctoral Science Foundation under Grant 2014M561291. (Corresponding author: Hong Chen.)

The authors are with the State Key Laboratory of Automotive Simulation and Control as well as Department of Control Science and Engineering, Jilin University, Changchun 130025, China (e-mail: wangyulei@jlu.edu.cn; yushuyou@126.com; yuanjingxinhuifei@163.com; chenh@jlu.edu.cn).

Color versions of one or more of the figures in this paper are available online at <http://ieeexplore.ieee.org>.

Digital Object Identifier 10.1109/TMECH.2018.2837128

R_e	Tire effective rolling radius.
V_x	Vehicle longitudinal speed at center of gravity.
V_{rx}	Vehicle longitudinal speed reference.
V_y	Vehicle lateral speed at center of gravity.
Ω_z	Vehicle yaw rate.
Ω_{rz}	Vehicle yaw rate reference.
l_f	Distance from front axle to the center of gravity.
l_r	Distance from rear axle to the center of gravity.
l_s	Half of the track width.
ω_i	Wheel rotational speed of the i th wheel.
T_i	Motor torque of the i th in-wheel motor.
k_i	Control gain of the i th in-wheel motor.
u_i	Control signal of the i th in-wheel motor.
δ	Ground-wheel steering angle.
δ_h	Hand-wheel steering angle.
μ	Tire-road friction coefficient.
ΔM_z	Additional yaw moment generated with the longitudinal tire force difference.

I. INTRODUCTION

MAXIMUM safety and minimum energy expense with comfort characterizes the definition of ideal human mobility. To realize this goal, a shared and intelligent driving is needed between the driver and the automat to realize braking, powertrain and steering control. This involves the novel vehicular cyber-physical and human system [1] with in-wheel motor (IWM) driven electric ground vehicles (EGVs) [2]–[4], X-by-Wire systems [5]–[7], advanced driving assistance systems (ADAS) [8], [9] and intelligent transportation systems (ITS) [10]. These promising techniques have promoted the development of intelligent lateral and longitudinal autonomous feedback control in electric vehicles [11], [12]. Consequently, a completely new and expanded architecture emerges, where the IWM EGVs are able to cooperate with the novel mechatronics systems and ITS information to generate a safe motion control vector for human mobility.

In this automotive architecture, a high level penetration of information and electric technologies have emerged. However, these electric systems are often prone to be inoperative and in case of failure, the criticality is high. It implies that the failures should be diagnosed and automatically corrected in real time. A large number of research work have been carried out in the area of fault detection and isolation (FDI) and fault-tolerant control (FTC) (see, e.g., [13]–[16]). As for application, A significant amount of research has been done to report the FDI/FTC

problem of IWM EGVs. To mention a few, in [17], the yaw control issue for IWM EGVs based on the differential steering mechanism was investigated when the regular active steering system is out of control, but it is not applicable to longitudinal control. To solve this problem, authors [18] introduced an adaptive control law with recursive least-square estimator to control longitudinal speed and yaw rate, and allocate the torque of each in-wheel motor, while the effect of lateral stability is overlooked. For the integrated FTC problem, the integrated fault-tolerant controller based on linear parameter-varying (LPV) techniques was developed by [11] to achieve the simultaneous lateral and longitudinal autonomous motion under moderate faults in-wheel motors and/or steering systems. However, the control performance is limited by the polytopes assumptions and the linearized models. Actually, it is generally hard to converge the three errors (i.e., longitudinal error, lateral offset and yaw error) due to vehicle nonlinearity and the high-level requirement in transient response.

In addition, in all those works, it was assumed that the FTC test procedures of concern are not actually driver-in-the-loop, which means the effects of a driver in the driving loop are not taken into consideration and not fully explored. To address this issue, both driver modeling and supervisory control of human-machine interaction are investigated. A comprehensive survey of driver modeling is presented in [19]. Both linear quadratic preview and model predictive control (MPC) approaches have been shown to be effective for the path-following task. In [20], driver and vehicle controllers were defined as two players in a dynamic game for maximizing stability of vehicle. In [21], an in-vehicle eco-driving assistance system was developed for coaching drivers towards the effective response on the usage of accelerator and braking pedals. In [22], online identification of driver behavior was used to generate a time-varying driving model and applied it in the overall direct yaw control scheme. As a result, an interesting question would be whether we can develop a kind of control approach and feedback methodology to address the FTC problem of electric ground vehicles under the driver-in-the-loop, and further to provide several additional functions on driving guidance, monitoring and evaluation [23].

This paper focuses on the development of a driver-in-the-loop FTC scheme that can achieve both the motion objective of EGVs and the driving guidance, monitoring and evaluation in the presence of different types of actuator faults, parameter uncertainties, disturbances and different driving behaviors. The main contributions of the paper are listed as follows.

- 1) Two parallel and independent models are investigated. The former describes the dynamics of IWM EGVs with the potential faults, while the latter responses to a virtual reference model mainly presenting the expected driving behaviors.
- 2) The simultaneous longitudinal, lateral and yaw control for IWM EGVs under actuator faults is supported based on a triple-step nonlinear controller [24] with on-line updating laws, and thus dangerous consequences for vehicles can be avoided.

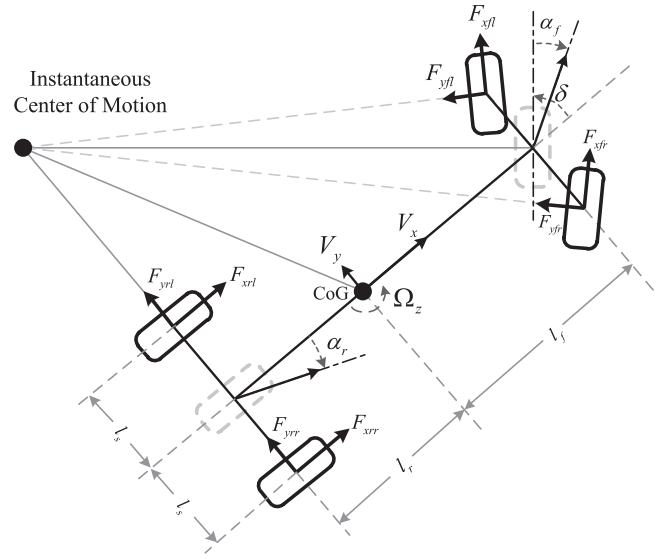


Fig. 1. Schematic of vehicle models.

- 3) Parameter uncertainties for the inertias and the cornering stiffness are considered to make vehicle robust to different driving conditions.
- 4) Using the standard test procedure, a triple-step feedback strategy is then employed to generate a driving guidance signal vector on steering wheel and pedals.
- 5) With an MPC driver, the residual signal with threshold in the FDI domain is now utilized for monitoring and evaluating drivers with different weighting coefficients.

The rest of this paper is organized as follows. The vehicle dynamics on the longitudinal, lateral and yaw motions, state space model, parameter uncertainties, fault models, reference model and problem formulation are described in Section II. The triple-step nonlinear approach-based fault-tolerant control law and the issues of driver guidance, monitoring and evaluation are proposed in Section III. Simulation based on veDYNA Simulink platform using a high-fidelity and full-vehicle model is conducted in Section IV.

II. SYSTEM MODELING AND PROBLEM FORMULATION

A. Vehicle Dynamics

Ignoring the pitch and roll motions, the vehicle has three planar degrees of freedom for the longitudinal, lateral and yaw motions. A schematic of the vehicle model shown in Fig. 1 is adopted to model the vehicle longitudinal, lateral and yaw motions.

Considering the external yaw moment ΔM_z generated with the longitudinal tire force differences between the left and right wheels, the vehicle can be modeled as [3]

$$\begin{cases} \dot{V}_x = V_y \Omega_z - \frac{C_a}{M} V_x^2 + \frac{1}{M} F_X \\ \dot{V}_y = -V_x \Omega_z + \frac{1}{M} (F_{yf} \cos \delta + F_{yr}) \\ \dot{\Omega}_z = \frac{1}{I_z} (l_f F_{yf} \cos \delta - l_r F_{yr}) + \frac{1}{I_z} \Delta M_z \end{cases} \quad (1)$$

where V_x and V_y are the longitudinal speed and lateral speed, respectively, Ω_z is the yaw rate, M is the mass of the vehicle, I_z is the vehicle yaw inertia, C_a is the aerodynamic drag term, and the external yaw moment can be calculated as [11]

$$\Delta M_z = (F_{xfr} \cos \delta + F_{xrr})l_s - (F_{xfl} \cos \delta + F_{xrl})l_s. \quad (2)$$

The front and rear lateral forces can be written as

$$F_{yf} = F_{yfl} + F_{yfr}, \quad F_{yr} = F_{yrl} + F_{yrr} \quad (3)$$

with F_{yi} being the lateral tire force of the i th wheel, and the total longitudinal force F_X generated by all the four tires can be calculated by

$$F_X = (F_{xfl} + F_{xfr}) \cos \delta + F_{xrl} + F_{xrr} - (F_{yfl} + F_{yfr}) \sin \delta. \quad (4)$$

On the assumption of the small sideslip angles, the front and rear lateral forces can be modeled as the following linear models [2]:

$$F_{yf} = C_f \alpha_f, \quad F_{yr} = C_r \alpha_r \quad (5)$$

where $C_{f,r}$ are the tire cornering stiffness values and $\alpha_{f,r}$ are the tire slip angles that can be expressed as [11]

$$\alpha_f = \delta - \frac{V_y}{V_x} - \frac{\Omega_z l_f}{V_x}, \quad \alpha_r = \frac{\Omega_z l_r}{V_x} - \frac{V_y}{V_x}. \quad (6)$$

The rotational dynamics of each wheel is represented by

$$I \dot{\omega}_i = -R_e F_{xi} + T_i \quad (7)$$

where I is the wheel moment of inertia, R_e is the tire effective rolling radius, and T_i is the torque of the i th in-wheel motor. If an in-wheel motor and its driver are treated as a unit, then the motor driver and in-wheel motor unit can be described by a control gain k_i , which is defined as

$$T_i = k_i u_i \quad (8)$$

where u_i with $i \in \{fl, fr, rl, rr\}$ is the torque control signal to the motor's driver.

B. State Space Model and Disturbances

Note that two control efforts on the same side of the vehicle have similar effects on the vehicle lateral and yaw motions. When the vehicle is under healthy condition, one has $k_{fl} = k_{fr} = k_{rl} = k_{rr} = k_0$ with k_0 being the nominal control gain of the healthy motor. Therefore, after denoting δ as an input, a straightforward motor signal allocation is to make the two motors on the same side of the vehicle have the identical signal and denote that

$$u_{fl} = u_{rl} = u_1, \quad \delta = u_2, \quad u_{fr} = u_{rr} = u_3. \quad (9)$$

The state space vehicle model with external disturbances can further be written as

$$\begin{aligned} \dot{V}_x &= V_y \Omega_z - \frac{C_a}{M} V_x^2 + \frac{k_{fl} + k_{rl}}{MR_e} u_1 + \frac{k_{fr} + k_{rr}}{MR_e} u_3 + \bar{d}_1 \\ \dot{V}_y &= -\frac{C_f + C_r}{M} \frac{V_y}{V_x} - V_x \Omega_z + \frac{C_r l_r - C_f l_f}{M} \frac{\Omega_z}{V_x} \\ &\quad + \frac{C_f}{M} u_2 + \bar{d}_2 \\ \dot{\Omega}_z &= \frac{C_r l_r - C_f l_f}{I_z} \frac{V_y}{V_x} - \frac{C_f l_f^2 + C_r l_r^2}{I_z} \frac{\Omega_z}{V_x} + \frac{l_s (k_{fl} + k_{rl})}{I_z R_e} u_1 \\ &\quad + \frac{C_f l_f}{I_z} u_2 - \frac{l_s (k_{fr} + k_{rr})}{I_z R_e} u_3 + \bar{d}_3 \end{aligned} \quad (10)$$

where $\bar{d}_{1,2,3}$ can be expressed as

$$\begin{aligned} \bar{d}_1 &= \frac{1}{M} F_{yf} \sin \delta + \frac{1}{MR_e} (T_{fl} + T_{fr}) (\cos \delta - 1) \\ &\quad + \frac{I}{MR_e} [\cos \delta \quad \cos \delta \quad 1 \quad 1] \dot{\omega} \\ \bar{d}_2 &= \frac{1}{MV_x} F_{yf} (\cos \delta - 1) \\ \bar{d}_3 &= \frac{l_f}{I_z} F_{yf} (\cos \delta - 1) + \frac{l_s}{I_z R_e} (T_{fl} + T_{fr}) (\cos \delta - 1) \\ &\quad + \frac{l_s I}{I_z R_e} [\cos \delta \quad -\cos \delta \quad 1 \quad 1] \dot{\omega} \end{aligned} \quad (11)$$

where $\omega = [\omega_{fl} \quad \omega_{fr} \quad \omega_{rl} \quad \omega_{rr}]^T$.

Remark 1: In this paper, the fault-tolerant controller of vehicle motion is mainly designed for the normal driving condition, in which both terms $\cos \delta - 1$ and $\sin \delta$ are set to be disturbances. In addition, due to measurement noise, a straightforward way of using the time derivative of wheel angular speed signals maybe challenging. As $\dot{\omega}_i$ is usually small in normal driving, it is reasonable to omit its value in the modeling but place into the disturbance terms.

Remark 2: As for extreme driving conditions, e.g., obstacle avoidance maneuver [25] or tire blow-out [26] at high speed, more precise modeling for vehicle dynamics relies on a number of different assumptions. Hence, more works are expected in future for the design of an FT controller considering both faults and extreme driving conditions.

Remark 3: Referring to [18], [11], the longitudinal and lateral speeds V_x , V_y and the vehicle yaw rate Ω_z are assumed to be directly measured by GPS and inertia measurement to ensure the availability of state feedback control.

C. Model Uncertainties

One source of model uncertainties results from the change of road conditions and vehicle states. The vehicle mass M may change due to the payload change. Assuming M is bounded by its minimum values M_{\min} and its maximum value M_{\max} , then M can be represented by $M = M_0 + N(t) \tilde{M}$. According to [27], the moment of inertia is proportional to the mass, thus, the uncertain moment of inertia can be written as $I_z = k_I^2 M_0 + N(t) k_I^2 \tilde{M}$, where k_I^2 is relevant coefficient between the mass and the moment of inertia.

Another kind of significant model uncertainty is induced by the tire nonlinearity. Normally, the tire cornering stiffness is treated as known constant parameter to facilitate the controller design. Nevertheless, it should be important to note that the tire cornering stiffness can be affected by many factors such as the normal vertical force, slip angle. Significant research has been done to report this problem. To mention a few, in [11] the preselected cornering stiffness is considered to be inaccurate and the gain scheduled control is designed by solving linear matrix inequality. In [28], the tire cornering stiffness is approximated by piecewise affine functions, whereas in [29], the tire force characteristics are approximated by a nonlinear function. For a tradeoff between modeling complexity and control flexibility, we are going to give the nominal value of the tire cornering stiffness and deal with its uncertainty by adaptive techniques.

D. Fault Model

If an actuator fault occurs, the actual control torque signal T_i from the actuator will be different to its desired one. In this paper, the three most common types of actuator faults, i.e., loss-of-effectiveness fault, additive fault, and the fault makes an actuator control effect stuck-at-fixed-level are studied. To model all of these fault types in a generalized way, let us introduce the following actuator fault model:

$$u_i = \eta_i u_{di} + \Delta u_i \quad (12)$$

with $i = \{fl, fr, rl, rr, s\}$. Note that u_{di} are the desired control effort of actual actuators, $0 \leq \eta_i \leq 1$ are time-varying parameters depending on the loss of effectiveness, and Δu_i are unknown disturbances caused by the additive and/or stuck faults. For example, if an additive fault occurs to an in-wheel motor, we have $\eta_i = 1$ and $\Delta u_i \neq 0$. If a loss-of-effectiveness fault occurs, we have $\eta_i < 1$ and $\Delta u_i = 0$. Similarly, the case $\eta_i = 0$ and $\Delta u_i = c$ with c being a constant describes the actuator stuck at a fixed level. Note that $\eta_i = 1$ and $\Delta u_i = 0$ means the healthy model.

E. Reference Model

The objective of a driving model is to provide the desired trajectory as the reference for vehicle motion control. Hence, the driving model for the desired longitudinal speed V_{rx} can be written as

$$\dot{V}_{rx} = k_x a_x \quad (13)$$

where k_x is a constant gain and a_x is the vehicle acceleration that is related to the accelerator/brake pedal position.

It is known that a zero vehicle lateral velocity can keep vehicle side slip angle zero that should be contained to improve vehicle stability [11]. So the reference vehicle lateral velocity is set to be zero, i.e., $V_{ry} = 0$.

In driving model, the desired vehicle yaw rate Ω_{rz} should be a function of the driver's steering wheel angle and vehicle speed. Referring to [11], its dynamics can be given by

$$\dot{\Omega}_{rz} = -k_\omega \Omega_{rz} + k_\omega f(V_{rx}) \delta_h \quad (14)$$

where $f(V_{rx}) = G_r k_a V_{rx} / (k_b V_{rx}^2 l + l)$, k_ω is a time constant, l is the vehicle wheel base, k_a is the gain of the reference model,

k_b is the stability factor, and G_r is the gear ratio of the steering mechanism linkage.

Denoting a vector $v = [v_1 \ v_2]^T = [a_x \ \delta_h]^T$ consisting of the driver action, the driving model can be summarized as

$$\begin{aligned} \dot{V}_{rx} &= k_x v_1 \\ \dot{\Omega}_{rz} &= -k_\omega \Omega_{rz} + k_\omega f(V_{rx}) v_2 \end{aligned} \quad (15)$$

F. Problem Formulation

Let a smooth and bounded longitudinal velocity V_{vx} and yaw rate reference Ω_{vz} be determined as the reference motion, given any initial states, the design objective is to develop, on one hand, a control law for $u = [u_1 \ u_2 \ u_3]^T$ such that the system in (10) is robustly asymptotically stable with disturbance attenuation performance in the presence of parameter uncertainties and unexpected actuator faults, and on the other hand, a real-time guidance law $v_r = [a_{rx} \ \delta_{rh}]^T$ and a residual J with threshold J_{th} that can be used to guide, monitor and evaluate the driver's driving behavior.

III. FAULT TOLERANT CONTROL DESIGN WITH DRIVER-IN-THE-LOOP

In this section, we first develop a triple-step method-based fault-tolerant control scheme for the case of the generalized actuator faults, uncertainties and external disturbances. Then, the result is extended to the driver-in-the-loop design.

A. Triple-Step Nonlinear Controller Design for FTC

The main idea of robust triple-step method can be demonstrated as follows. To simplify the tedious symbols mentioned above, it is general to denote the following lumped parameters $\theta_1 = -C_a/M$, $\theta_2 = -(C_f + C_r)/M$, $\theta_3 = (C_r l_r - C_f l_f)/M$, $\theta_4 = (C_r l_r - C_f l_f)/I_z$, $\theta_5 = -(C_f l_f^2 + C_r l_r^2)/I_z$, $\theta_6 = (\eta_{fl} k_{fl} + \eta_{fr} k_{fr})/(MR_e)$, $\theta_7 = (\eta_{fr} k_{fr} + \eta_{rl} k_{rl})/(MR_e)$, $\theta_8 = C_f \eta_s/M$, $\theta_9 = l_s (\eta_{fl} k_{fl} + \eta_{fr} k_{fr})/(I_z R_e)$, $\theta_{10} = (C_f l_f \eta_s)/I_z$, $\theta_{11} = -l_s (\eta_{fr} k_{fr} + \eta_{rl} k_{rl})/(I_z R_e)$, and replace u_d with u to facilitate reading. Then, the entire control-oriented model with the possible faults can be written as

$$\begin{aligned} \dot{V}_x &= V_y \Omega_z + \theta_1 V_x^2 + \theta_6 u_1 + \theta_7 u_3 + d_1 \\ \dot{V}_y &= \theta_2 \frac{V_y}{V_x} - V_x \Omega_z + \theta_3 \frac{\Omega_z}{V_x} + \theta_8 u_2 + d_2 \\ \dot{\Omega}_z &= \theta_4 \frac{V_y}{V_x} + \theta_5 \frac{\Omega_z}{V_x} + \theta_9 u_1 + \theta_{10} u_2 + \theta_{11} u_3 + d_3 \end{aligned} \quad (16)$$

where $d = [d_1 \ d_2 \ d_3]^T$ presents the generalized disturbance including faults, i.e.,

$$\begin{aligned} d_1 &= \bar{d}_1 + \frac{k_{fl} \Delta u_{fl} + k_{rl} \Delta u_{rl} + k_{fr} \Delta u_{fr} + k_{tr} \Delta u_{tr}}{MR_e} \\ d_2 &= \bar{d}_2 + \frac{C_f \Delta u_s}{M} \\ d_3 &= \bar{d}_3 + \frac{l_s (k_{fl} \Delta u_{fl} + k_{rl} \Delta u_{rl} - k_{fr} \Delta u_{fr} - k_{tr} \Delta u_{tr})}{I_z R_e} \end{aligned}$$

Since these lumped parameters θ_i maybe unknown due to parameter uncertainties ($C_{f,r}$, M , I_z) and the possible faults in (12), let us define $\hat{\theta}_i(t)$, $i = 1, \dots, 11$ standing for the estimates of these parameters at time t and design a controller as follows.

Step 1 Steady-state control: Inspired by the look-up tables based control that widely used in automotive engineering but to reduce the calibration effort, the alternative steady-state control is developed as u_s while retaining the basic function of the conventional loop-up tables. For (10) without disturbances, all the transient dynamics $\dot{x} = 0$. Consequently, the steady state control is obtained as

$$u_s = \begin{bmatrix} \hat{\theta}_6 & 0 & \hat{\theta}_7 \\ 0 & \hat{\theta}_8 & 0 \\ \hat{\theta}_9 & \hat{\theta}_{10} & \hat{\theta}_{11} \end{bmatrix}^{-1} \begin{bmatrix} -V_y \Omega_z - \hat{\theta}_1 V_x^2 \\ V_x \Omega_z - \hat{\theta}_2 \frac{V_y}{V_x} - \hat{\theta}_3 \frac{\Omega_z}{V_x} \\ -\hat{\theta}_4 \frac{V_y}{V_x} - \hat{\theta}_5 \frac{\Omega_z}{V_x} \end{bmatrix}. \quad (17)$$

Step 2 Reference variation based feed-forward control: Retaining the steady state control, we augment the control as $u = u_s + u_f$. Since it is necessary for a fast transient response, by enforcing $\dot{V}_x = \dot{V}_{rx}$, $\dot{V}_y = \dot{V}_{ry}$, and $\dot{\Omega}_z = \dot{\Omega}_{tz}$, the control u_f therefore is derived as

$$u_f = \begin{bmatrix} \hat{\theta}_6 & 0 & \hat{\theta}_7 \\ 0 & \hat{\theta}_8 & 0 \\ \hat{\theta}_9 & \hat{\theta}_{10} & \hat{\theta}_{11} \end{bmatrix}^{-1} \begin{bmatrix} \dot{V}_{rx} \\ \dot{V}_{ry} \\ \dot{\Omega}_{tz} \end{bmatrix}. \quad (18)$$

Step 3 Tracking error feedback control: Following Step 1 and Step 2, it is direct to impose the path tracking by completing the control law $u = u_s + u_f + u_e$ with a feedback control u_e . Define the tracking errors as $e_1 = V_{rx} - V_x$, $e_2 = V_{ry} - V_y$, and $e_3 = \Omega_{tz} - \Omega_z$. In order to the tracking objective, one can choose a nonlinear proportional-integral feedback control as

$$u_e = \begin{bmatrix} \hat{\theta}_6 & 0 & \hat{\theta}_7 \\ 0 & \hat{\theta}_8 & 0 \\ \hat{\theta}_9 & \hat{\theta}_{10} & \hat{\theta}_{11} \end{bmatrix}^{-1} \begin{bmatrix} k_1 e_1 + k_{01} \int e_1 dt \\ k_2 e_2 + k_{02} \int e_2 dt \\ k_3 e_3 + k_{03} \int e_3 dt \end{bmatrix}. \quad (19)$$

Then substituting the triple-step control law (17), (18), and (19) into the model (16) deduces that

$$\begin{aligned} \begin{bmatrix} \dot{V}_x \\ \dot{V}_y \\ \dot{\Omega}_z \end{bmatrix} &= \begin{bmatrix} \dot{V}_{rx} \\ \dot{V}_{ry} \\ \dot{\Omega}_{tz} \end{bmatrix} + \begin{bmatrix} V_y \Omega_z + \theta_1 V_x^2 \\ -V_x \Omega_z + \theta_2 \frac{V_y}{V_x} + \theta_3 \frac{\Omega_z}{V_x} \\ \theta_4 \frac{V_y}{V_x} + \theta_5 \frac{\Omega_z}{V_x} \end{bmatrix} \\ &- \begin{bmatrix} V_y \Omega_z + \hat{\theta}_1 V_x^2 \\ -V_x \Omega_z + \hat{\theta}_2 \frac{V_y}{V_x} + \hat{\theta}_3 \frac{\Omega_z}{V_x} \\ \hat{\theta}_4 \frac{V_y}{V_x} + \hat{\theta}_5 \frac{\Omega_z}{V_x} \end{bmatrix} + \begin{bmatrix} k_1 e_1 \\ k_2 e_2 \\ k_3 e_3 \end{bmatrix} + \begin{bmatrix} d_1 \\ d_2 \\ d_3 \end{bmatrix} \\ &- \left(\begin{bmatrix} \hat{\theta}_6 & 0 & \hat{\theta}_7 \\ 0 & \hat{\theta}_8 & 0 \\ \hat{\theta}_9 & \hat{\theta}_{10} & \hat{\theta}_{11} \end{bmatrix} - \begin{bmatrix} \theta_6 & 0 & \theta_7 \\ 0 & \theta_8 & 0 \\ \theta_9 & \theta_{10} & \theta_{11} \end{bmatrix} \right) \begin{bmatrix} u_1 \\ u_2 \\ u_3 \end{bmatrix}. \end{aligned}$$

Then, it holds that

$$\begin{aligned} \dot{e}_1 &= -k_1 e_1 - k_{01} \chi_1 - d_1 + V_x^2 \tilde{\theta}_1 + u_1 \tilde{\theta}_6 + u_3 \tilde{\theta}_7 \\ \dot{e}_2 &= -k_2 e_2 - k_{02} \chi_2 - d_2 + \frac{V_y}{V_x} \tilde{\theta}_2 + \frac{\Omega_z}{V_x} \tilde{\theta}_3 + u_2 \tilde{\theta}_8 \\ \dot{e}_3 &= -k_3 e_3 - k_{03} \chi_3 - d_3 + \frac{V_y}{V_x} \tilde{\theta}_4 + \frac{\Omega_z}{V_x} \tilde{\theta}_5 + \sum_{i=1}^3 u_i \tilde{\theta}_{8+i} \end{aligned}$$

where $\chi_i = \int e_i dt$ and $\tilde{\theta}_j = \hat{\theta}_j - \theta_j$.

Since the knowledge on $\tilde{\theta}_i$ or θ_i cannot be obtained exactly due to unexpected faults and uncertain parameters, the adaptive technique is employed to tackle this problem. In the following theorem, a parameter-independent robust triple-step nonlinear control scheme is developed for the purpose of fault-tolerant motion control.

Theorem 1: Consider the faulty system given by (16) without exact knowledge of θ_i . Select the triple-step control law $u = u_s + u_f + u_e$ given by (17), (18), and (19), Design k_i satisfying the following equations:

$$k_i = \frac{1}{2} \left(\lambda_i + \frac{1}{\gamma^2} \right), \lambda_i > 0, \gamma > 0 \quad (20)$$

and the updated law of

$$\begin{aligned} \dot{\hat{\theta}}_1 &= -\kappa_1 V_x^2 e_1, \quad \dot{\hat{\theta}}_2 = -\kappa_2 \frac{V_y}{V_x} e_2, \quad \dot{\hat{\theta}}_3 = -\kappa_3 \frac{\Omega_z}{V_x} e_2 \\ \dot{\hat{\theta}}_4 &= -\kappa_4 \frac{V_y}{V_x} e_3, \quad \dot{\hat{\theta}}_5 = -\kappa_5 \frac{\Omega_z}{V_x} e_3, \quad \dot{\hat{\theta}}_6 = -\kappa_6 u_1 e_1 \\ \dot{\hat{\theta}}_7 &= -\kappa_7 u_3 e_1, \quad \dot{\hat{\theta}}_8 = -\kappa_8 u_2 e_2, \quad \dot{\hat{\theta}}_9 = -\kappa_9 u_1 e_3 \\ \dot{\hat{\theta}}_{10} &= -\kappa_{10} u_2 e_3, \quad \dot{\hat{\theta}}_{11} = -\kappa_{11} u_3 e_3, \quad \kappa_1, \dots, \kappa_{11} > 0. \end{aligned} \quad (21)$$

Then, the closed-loop system satisfies the following:

- 1) *Disturbance Attenuation:* For any initial condition the following quadratic performance criterion is achieved:

$$\int_0^\infty \|e\|_Q^2 dt \leq \|e(0)\|^2 + \|\tilde{\theta}(0)\|_K^2 + \gamma^2 \int_0^\infty \|d\|^2 dt \quad (22)$$

where $Q = \text{diag}\{\lambda_1, \lambda_2, \lambda_3\}$ and $K^{-1} = \text{diag}\{\kappa_1, \dots, \kappa_{11}\}$.

- 2) *Robustly Asymptotically Tracking:* If the disturbance is bounded with finite energy and amplitude, i.e., $d \in \mathcal{L}_2[0, \infty) \cap \mathcal{L}_\infty[0, \infty)$, then $\lim_{t \rightarrow \infty} e(t) = 0$ and $\lim_{t \rightarrow \infty} \dot{e}(t) = 0$.

Proof: Choose the Lyapunov function candidate as

$$V = \sum_{i=1}^3 \frac{1}{2} e_i^2 + \sum_{i=1}^3 \frac{k_{0i}}{2} \chi_i^2 + \sum_{j=1}^{11} \frac{1}{2\kappa_j} \tilde{\theta}_j^2. \quad (23)$$

Taking the time derivative of V along the error dynamics and canceling unknown parameters and integral terms, we have

$$\begin{aligned}
\dot{V} &= \sum_{i=1}^3 e_i (-k_i e_i - k_{0i} \chi_i - d_i) + \sum_{i=1}^3 k_{0i} \chi_i e_i + \sum_{j=1}^{11} \frac{1}{2\kappa_j} \tilde{\theta}_j \dot{\hat{\theta}}_j \\
&+ e_1 (V_x^2 \tilde{\theta}_1 + u_1 \tilde{\theta}_6 + u_3 \tilde{\theta}_7) + e_2 \left(\frac{V_y}{V_x} \tilde{\theta}_2 + \frac{\Omega_z}{V_x} \tilde{\theta}_3 + u_2 \tilde{\theta}_8 \right) \\
&+ e_3 \left(\frac{V_y}{V_x} \tilde{\theta}_4 + \frac{\Omega_z}{V_x} \tilde{\theta}_5 + u_1 \tilde{\theta}_9 + u_2 \tilde{\theta}_{10} + u_3 \tilde{\theta}_{11} \right) \\
&= - \sum_{i=1}^3 e_i (k_i e_i + d_i) = - \sum_{i=1}^3 e_i \left(\frac{1}{2} \left(\lambda_i + \frac{1}{\gamma^2} \right) e_i + d_i \right) \\
&= - \frac{1}{2} e^T Q e - \frac{1}{2} \left(\frac{1}{\gamma} e + \gamma d \right)^T \left(\frac{1}{\gamma} e + \gamma d \right) + \frac{1}{2} \gamma^2 d^T d \\
&\leq - \frac{1}{2} e^T Q e + \frac{1}{2} \gamma^2 d^T d. \tag{24}
\end{aligned}$$

Integrating the above inequality from $t = 0$ to ∞ leads to (22), and if $d \in \mathcal{L}_2[0, \infty) \cap \mathcal{L}_\infty[0, \infty)$, using the Barbalat's lemma, then the performance of robustly asymptotically tracking holds. ■

Remark 4: The proposed robust adaptive triple-step nonlinear control law not only inherits the merits of the conventional triple-step nonlinear method [24], such as the engineering idea of the step-by-step design, the compatibility of lookup table, the zero-offset for impulse and step disturbances, but also provides the adaptability and a quantified guideline for tuning parameter $k_{1,2,3}$, which guarantees the H_∞ tracking offset for arbitrary bounded disturbances.

Remark 5: The control law in Theorem 1 can only guarantee the convergence of tracking error, while the parameter convergence maybe not taken care of because the persistent excitation does not always hold during the closed-loop operation. It should be emphasized that it is the entire triple-step control scheme rather than solo adaptive law that tolerates the actuator faults of electric ground vehicles.

Remark 6: Besides, an adaptive control-based FTC for IWM EGVs has been published in [18]. However, compared with [18], the proposed approach includes some new features, such as the coordinated triple-step nonlinear control for the lateral stability, the generalized adaptive laws updating more parameters, the driver-in-the-loop design with the driver guidance, monitoring and evaluation in the next section.

B. Triple-Step Feedback Guidance Design for Driving Monitoring and Evaluation

Note that the driving model (15) is given independently of vehicle dynamics in (16) and the reference motion trajectory is given as V_{vx} and Ω_{vz} . Then, it is straightforward from the triple-step idea to design a triple-step feedback guidance $v_r = v_{rs} + v_{rf} + v_{re}$ as follows.

Step 1: Steady-state guidance

$$v_{rs} = \begin{bmatrix} 0 \\ \frac{1}{f(V_{rx})} \Omega_{rz} \end{bmatrix}. \tag{25}$$

Step 2: Reference variation based feed-forward guidance

$$v_{rf} = \begin{bmatrix} \frac{1}{k_x} & 0 \\ 0 & \frac{1}{k_\omega f(V_{rx})} \end{bmatrix} \begin{bmatrix} \dot{V}_{vx} \\ \dot{\Omega}_{vz} \end{bmatrix}. \tag{26}$$

Step 3: Tracking error feedback guidance

$$v_{re} = \begin{bmatrix} \frac{1}{k_x} & 0 \\ 0 & \frac{1}{k_\omega f(V_{rx})} \end{bmatrix} \begin{bmatrix} k_{r1} e_{r1} + k_{r01} \int e_{r1} dt \\ k_{r2} e_{r2} + k_{r02} \int e_{r2} dt \end{bmatrix} \tag{27}$$

where $e_{r1} = V_{vx} - V_{rx}$ and $e_{r2} = \Omega_{vz} - \Omega_{rz}$.

In order to mimic the test procedure and perform the driver-in-the-loop simulation, the driver model should be considered. According to [19] and [30], there are mainly two components characterizing the driver driving response: the stretch and passive response of neuromuscular dynamics, and the cognitive response of the brain.

Based on experimental tests [30], the response of neuromuscular dynamics can be modeled as a transfer function between the driving torque and the driving angle: $H_{4w}(s) = 1/(J_a s^2 + c_a s + k_a)$ where J_a is related to the driver inertia mainly involved in the vibration, while c_a and k_a describe a spring-like behavior at low frequency.

Compared with neuromuscular dynamics, the cognitive response of the brain is more complex. In this paper, we assume that the cognitive response is related to the path following task. From the viewpoint of the feed-forward and feedback control, the use of a receding horizon strategy, e.g., an MPC approach, is available since the reference v_r has been provided by the proposed triple-step guidance. Due to the space limitation, the design of an MPC driver is omitted.

It should be emphasized that the ratio between the input and output weighting factors, i.e., $\beta = W_y/W_u$, could potentially reflect the driving skill of a driver. Generally speaking, a higher ratio β indicates the driver a better vehicle path tracking by a higher driving effort. On the contrary, the driver could relax himself/herself or show fatigue, which can be also reflected by reducing β in the driver model.

Due to the driver behavior involved, vehicle driving safety is not just related to vehicle itself but the vehicle-human closed loop. Thereafter, real-time monitoring and evaluating the driver behavior becomes significant for driver-in-the-loop FTC. For this purpose, we are able to generate a residual by comparison of v_r with v :

$$J(s) = r^T(s) Q_r r(s), \quad r(s) = v_r(s) - v(s) \tag{28}$$

with a positive definite matrix Q_r (from the standard statistic test [13]) and set a threshold J_{th} that allows a reliable evaluation of the driver behavior. In our study, we shall establish a driving evaluation rule

$$J(s) > J_{th} \Rightarrow \text{Low attention driving.} \tag{29}$$

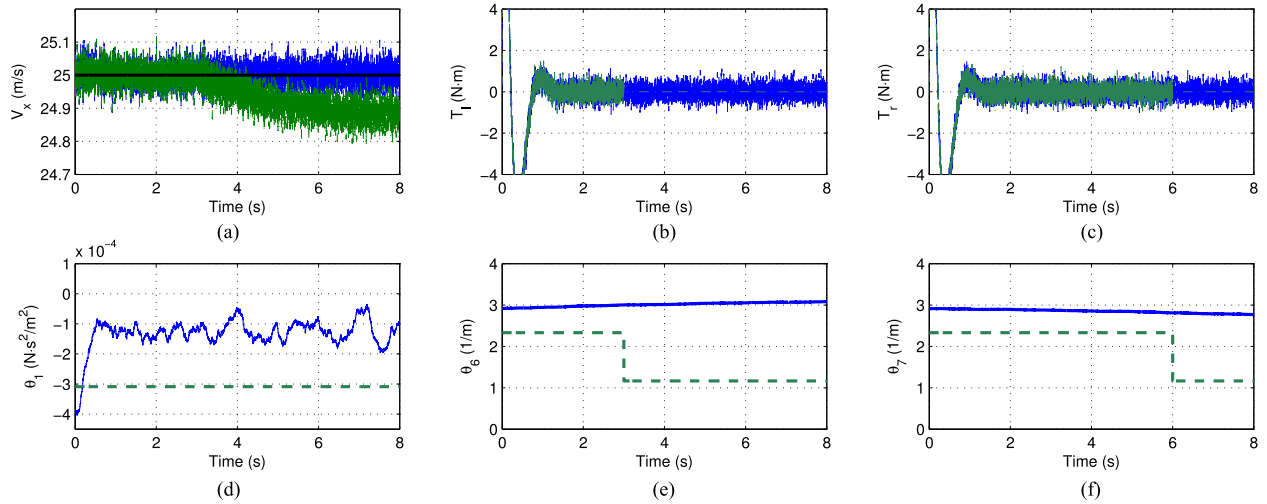


Fig. 3. Simulation results in the straight line case. (a) Vehicle longitudinal speeds. Black: reference; blue: controlled; green: uncontrolled. (b) Front-left motor torques. Blue: command value; green: actual value. (c) Rear-right motor torques. Blue: command value; green: actual value. (d) Parameter θ_1 . Blue: updated value; green: actual value. (e) Parameter θ_6 . Blue: updated value; green: actual value. (f) Parameter θ_7 . Blue: updated value; green: actual value.

not converge to their actual values. But the controlled speed as shown in Fig. 3(a) could verify the tracking performance of the proposed control scheme compared with the driver active correction one. To show the control feasibility, the commanded and actual motor torques of left and right motors are plotted in Fig. 3(b) and (c), respectively.

B. J-Turn Simulations

The vehicle runs at a low speed range and low friction surface with $\mu = 0.4$ in this simulation. The desired speed increases from 9 m/s to 13 m/s in 8 s, and the hand-wheel steering angle trajectory is selected as a typical counterclockwise turn [11]. In addition, as shown in Theorem 1, different values of the control gains in FTC scheme will lead to a different convergence speed and robustness, and these may also result in the different behavior of vehicle motion. Consequently, the gains for J-turn simulation are selected as $k_1 = 50$, $k_{01} = 100$, $k_2 = 20$, $k_{02} = 0$, $k_3 = 500$, and $k_{03} = 500$.

For the driver-in-the-loop simulation, three parameters $J_a = 0.094$, $c_a = 0.59$, and $k_a = 3.4$ in the neuromuscular model are given to represent a normal driver [19]. For the cognitive response of a driver, the sampling time is 1ms, the control and output predictive lengths are set to be 10 and 80, respectively. And two weighting ratios $\beta = 10$ ($W_y = 10$, $W_u = 1$) or 1 ($W_y = 1$, $W_u = 1$) are considered to imitate different driving behaviors, respectively.

Three different faults are sequentially applied in this test: At 4s, a loss-of-effectiveness fault occurs to the steering system and makes the control effectiveness of the steering system decrease to half of its desired value, which means $\delta_2 = 0.5\delta_d$; At 5 s, an additive fault occurred to the front-right in-wheel motor, which made the motor torque changed to $T_{fr} = T_{dfr} + \Delta T_{fr}$ with T_{dfr} being the desired torque and $\Delta T_{fr} = -20 - 10 \sin(t)$; At 7 s, a loss-of-effectiveness fault occurs to the rear-left in-wheel motor, which makes the actual motor torque decrease to 60% of its

desired value. To better show the performance of the proposed controller, the states of an uncontrolled vehicle with the same hand-wheel steering input and motor torque control signals are also plotted in the figures.

Fig. 4(a) shows vehicle longitudinal speeds under the driver-in-the-loop FTC scheme with weighting factors $\beta = 10$ and 1, respectively. One can see that both longitudinal speed trajectories of the controlled vehicle are close to the reference even if system uncertainties, disturbances and faults exist, whereas the longitudinal speed of the vehicle without control cannot follow the reference as soon as the faults are introduced. The similar conclusions can be made to the lateral speed and yaw rate results, which are plotted in Fig. 4(b) and (c). The actuator effects of steering angle and motor torques are shown in Fig. 4(d)–(f). Note that the lateral speed control result of the uncontrolled vehicle is smaller than that of the control one. This is because the uncontrolled vehicle could not make the turn as desired due to the actuator faults. The updated and actual values of θ_9 are plotted in Fig. 4(i). The vehicle global trajectories are compared in Fig. 4(g), where we can see that even through three different faults and human behaviors were injected, the vehicle could still track the reference well.

Fig. 4(h) shows different driver behaviors in the J-turn simulation. Using the triple-step design, the guidance for the J-turn is similar with a pulse signal. Observe that the MPC driver with $\beta = 10$ reveals a better path tracking ability to the triple-step guidance compared with the one with $\beta = 1$, and the latter could reflect himself/herself in relax or aggressive longitudinal driving. The similar conclusion can be observed to the hand-wheel steering result plotted in Fig. 4(i) although the periodic perturbation in the high frequency was contaminated by noise. However, as shown in Fig. 4(a)–(d), the difference between two drivers is hidden due to the bandwidth of the close-loop vehicle control. To avoid the potential risks caused by driver, a driver monitoring and evaluation system is designed to generate the residual

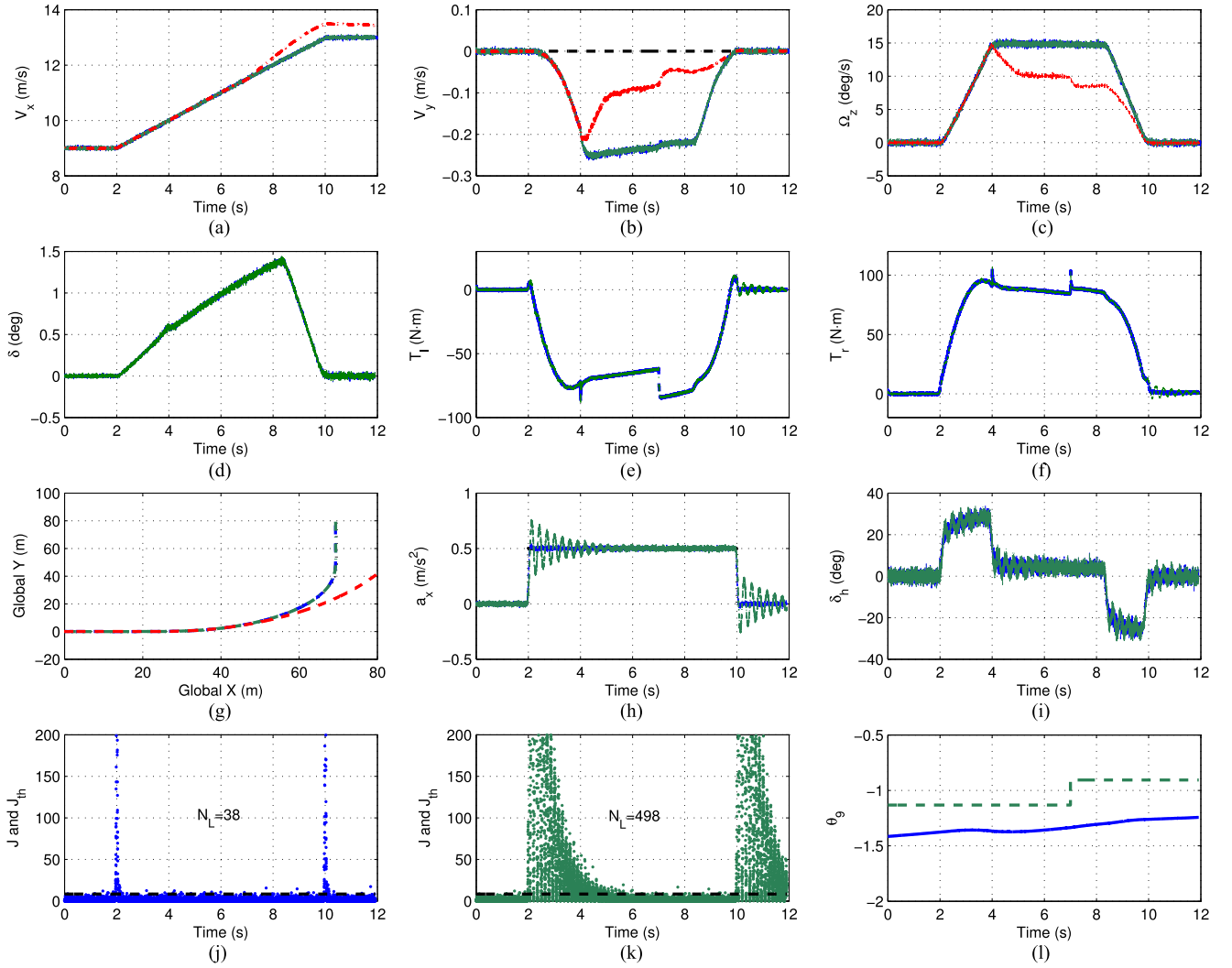


Fig. 4. Simulation results in the J-turn case. (a) Vehicle longitudinal speeds. Black: V_{vx} ; blue: controlled V_x with $\beta = 10$; green line: controlled V_x with $\beta = 1$; red line: V_x without control. (b) Vehicle lateral speeds. Black line: V_{vy} ; blue line: controlled V_y with $\beta = 10$; green line: controlled V_y with $\beta = 1$; red line: V_y without control. (c) Vehicle yaw rates. Black line: Ω_{vz} ; blue line: controlled Ω_z with $\beta = 10$; green line: controlled Ω_z with $\beta = 1$; red line: Ω_z without control. (d) Vehicle ground-wheel steering angles. Blue line: controlled δ with $\beta = 10$; green line: controlled δ with $\beta = 1$; red line: Ω_z without control. (e) Vehicle left-wheel torques. Blue line: controlled T_l with $\beta = 10$; green line: controlled T_l with $\beta = 1$. (f) Vehicle right-wheel torques. Blue line: controlled T_r with $\beta = 10$; green line: controlled T_r with $\beta = 1$. (g) Vehicle trajectories. Black line: reference trajectory; blue line: controlled trajectory with $\beta = 10$; green line: controlled trajectory with $\beta = 1$; red line: trajectory without control. (h) Driver accelerator/brake behaviors. Black line: accelerator/brake guidance v_{r1} ; blue line: driver accelerator/brake behavior v_1 with $\beta = 10$; green line: driver accelerator/brake behavior v_1 with $\beta = 1$. (i) Driver steering behaviors. Black line: steering guidance v_{r2} ; blue line: steering behavior v_2 with $\beta = 10$; green line: steering behavior v_2 with $\beta = 1$. (j) Residual sequence with $\beta = 10$. Blue dots: residual J with $\beta = 10$; black line: threshold. (k) Residual sequence with $\beta = 1$. Blue dots: residual J with $\beta = 1$; black line: threshold. (l) Parameter θ_9 . Blue line: updated value; green line: actual value.

signals and their thresholds, as shown in Fig. 4(j) and (k). One can see that the low attention index N_L of the driver with $\beta = 1$ is larger than that of N_L with $\beta = 10$, which could provide the possible evidence to remind driver, and even reconstruct vehicle control to fully-automated operation.

C. Single-Lane Change Simulations

In this simulation, the vehicle is controlled to make a single-line change at a high speed and high friction surface with $\mu = 0.8$. A driver model with parameters $J_a = 0.094$, $c_a = 1.12$, and $k_a = 59.6$ is selected to imitate a closed-loop maneuver together with a tense driver [19]. To eliminate the lateral error,

the gains for single-lane turn simulation are chosen as $k_1 = 50$, $k_{01} = 100$, $k_2 = 5$, $k_{02} = 50$, $k_3 = 500$, and $k_{03} = 500$. To verify the lateral safety with driver-in-the-loop, two weighting ratios $\beta = 10$ and $\beta = 0.5$ are considered to imitate different driver's steering behaviors, respectively.

Both the steering and in-wheel motor faults are introduced as follows: At 3 s, an additive fault and a loss-of-effectiveness fault are applied to steering system. These two faults make the actual ground-wheel steering angle change to $\delta = 0.6\delta_d - 3^\circ$; At 6 s, an in-wheel fault which makes the motor torque stuck at -20 N.m is introduced to the rear-left in-wheel motor.

The longitudinal speed control results are plotted in Fig. 5(a), which indicates the longitudinal speeds of the controlled faulty

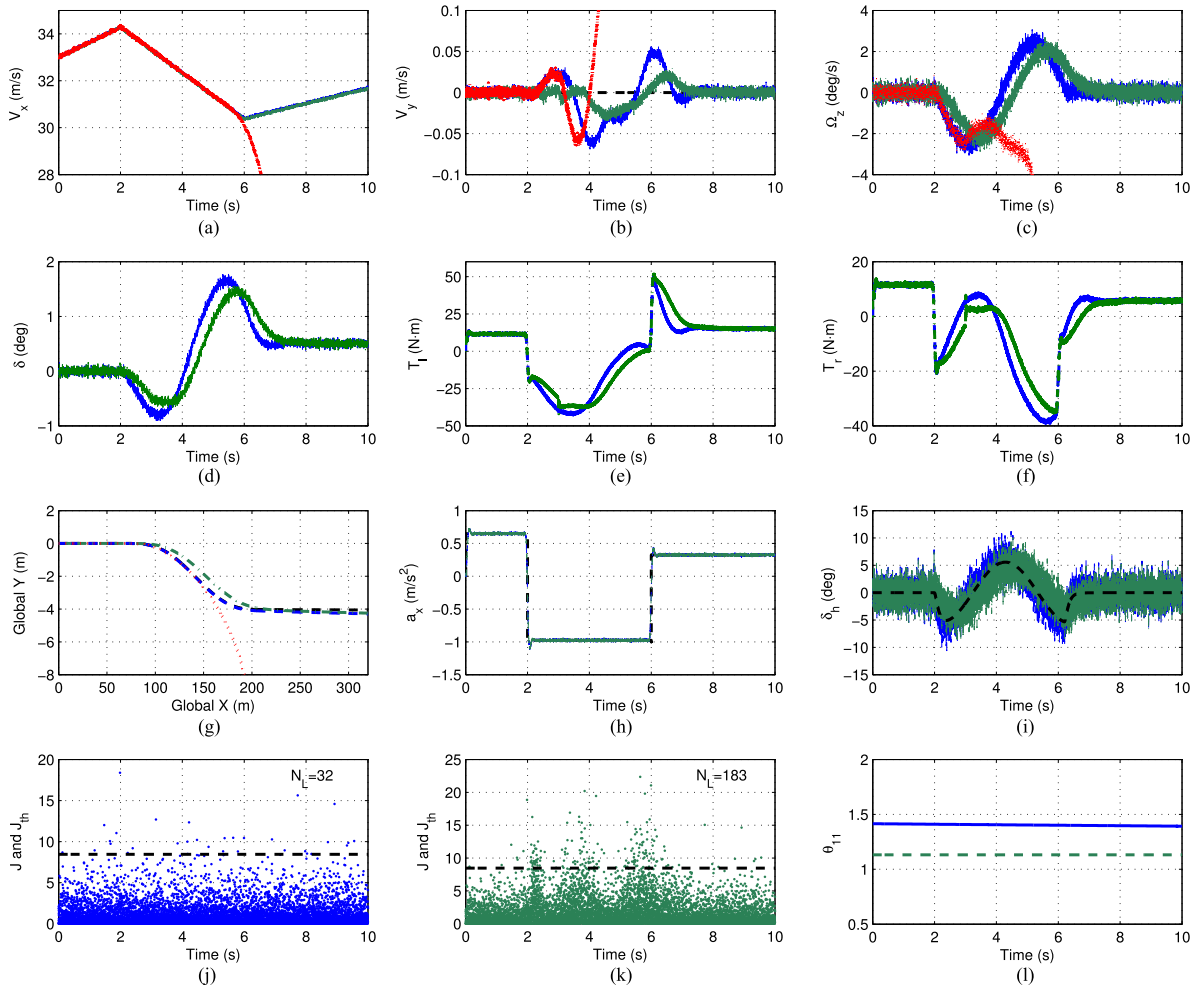


Fig. 5. Simulation results in the single-lane change case. (a) Vehicle longitudinal speeds. Black line: V_{vx} ; blue line: controlled V_x with $\beta = 10$; green line: controlled V_x with $\beta = 0.5$; red line: V_x without control. (b) Vehicle lateral speeds. Black line: V_{vy} ; blue line: controlled V_y with $\beta = 10$; green line: controlled V_y with $\beta = 0.5$; red line: V_y without control. (c) Vehicle yaw rates. Black line: Ω_{vz} ; blue line: controlled Ω_z with $\beta = 10$; green line: controlled Ω_z with $\beta = 0.5$; red line: Ω_z without control. (d) Vehicle ground-wheel steering angles. Blue line: controlled δ with $\beta = 10$; green line: controlled δ with $\beta = 0.5$. (e) Vehicle left-wheel torques. Blue line: controlled T_l with $\beta = 10$; green line: controlled T_l with $\beta = 0.5$. (f) Vehicle right-wheel torques. Blue line: controlled T_r with $\beta = 10$; green line: controlled T_r with $\beta = 0.5$. (g) Vehicle trajectories. Black line: reference trajectory; blue line: controlled trajectory with $\beta = 10$; green line: controlled trajectory with $\beta = 0.5$; red line: trajectory without control. (h) Driver accelerator/brake behaviors. Black line: accelerator/brake guidance v_{r1} ; blue line: accelerator/brake behavior v_1 with $\beta = 10$; green line: accelerator/brake behavior v_1 with $\beta = 0.5$. (i) Driver steering behaviors. Black line: steering guidance v_{r2} ; blue line: steering behavior v_2 with $\beta = 10$; green line: steering behavior v_2 with $\beta = 0.5$. (j) Residual sequence with $\beta = 10$. Blue dots: residual J with $\beta = 10$; black line: threshold. (k) Residual sequence with $\beta = 0.5$. Blue dots: residual J with $\beta = 0.5$; black line: threshold. (l) Parameter θ_{11} . Blue line: updated value; green line: actual value.

vehicles could follow the reference, whereas the one without FTC jumps and deviates from the desired trajectory due to actuator faults. The vehicle lateral speeds and yaw rates with control and without control are shown in Fig. 5(b) and (c), respectively. One can see from these two figures that both of variables could be well controlled when the driver provides a high driving effort. The updated and actual values of θ_{11} are plotted in Fig. 5(l). The actuator effects of steering angle and motor torques are shown in Fig. 5(d)–(f). The vehicle global trajectories are shown in Fig. 5(g), by which the effectiveness of the proposed FTC scheme can be verified.

To assist the driver efficient driving, both accelerator/brake and steering guidance are provided as shown in Fig. 5(h) and (i). One can observe that the driver with $\beta = 0.5$ cannot follow the steering reference well compared with the one with $\beta = 10$.

The obvious phenomenon is the steering delay during the lane change, which could reflect the driver's physiological fatigue. Accordingly, the longitudinal speed, the lateral speed, the yaw rate and the trajectory of the driver-in-the-loop vehicle control with the driver $\beta = 0.5$ are changed, as shown in Fig. 5(a)–(d). The steering delay may lead to an obstacle collision accident. Therefore, to benefit the avoidance maneuver, the residual signals are generated to monitor drivers, as shown in Fig. 5(i) and (k).

D. Comparison With the Existing FTC Schemes

For the purpose of comparison, the adaptive FTC proposed by [18] is applied to the double-lane change control under the fault-free and fault simulations without driver-in-the-loop. The

TABLE II
PERFORMANCE SUMMARY UNDER DIFFERENT CONTROL SCHEMES

Control Performance	Healthy Status	Control Schemes			
		TS-FTC (UA)	A-FTC	LPV-FTC	
\mathcal{L}_2 -Norm	Long	Normal	31.7 (35.5)	41.8	23.2
		Fault	21.1 (43.4)	29.2	19.2
	Lat	Normal	0.3 (0.2)	17.9	0.3
		Fault	2.1 (14.5)	44.1	11.8
	Yaw (e3)	Normal	1.1 (1.2)	0.7	0.8
		Fault	2.8 (7.1)	1.1	2.7
\mathcal{L}_∞ -Norm	Long (e-1)	Normal	1.3 (1.6)	1.3	1.4
		Fault	1.6 (1.8)	1.4	1.4
	Lat (e-2)	Normal	1.4 (1.8)	6.1	1.6
		Fault	3.4 (7.9)	12	7.1
	Yaw (e-1)	Normal	6.9 (11.4)	7.1	6.9
		Fault	12.0 (19.8)	7.1	13.0
STT (12s) $ e_y < 0.02$	Normal	12.0 (12.0)	6.5	12.0	
	Fault	10.8 (5.5)	5.0	8.6	

STT: Satisfactory Tracking Time. Long: longitudinal Acc.; Lat: lateral Acc.; Yaw: Yaw Rate; UA: The triple-step method without adaption.

control performance of the FT controllers is investigated in the case that all actuators decrease to half of their desired values. For a further comparison, the simulation is also conducted with the LPV control-based passive FT controller proposed by [11] under the above-mentioned two conditions: fault-free and the considered faulty scenario.

To gain more insight in a quantitative manner, the control performance is summarized in Table II to make the comparison more apparent. From the results in Table II, it is mentioned that, because of the nonlinear control structure and the adaptive law, the proposed TS-FTC scheme provides a better control performance in the lateral stability than A-FTC [18] and LPV-FTC [11] whenever actuator faults occur or not, which also means that our proposed control scheme can be appealing to realize the motion control of electric vehicles with a high lateral stability. To show the usefulness of parameter adaption, the control performance indexes of a triple-step control scheme without adaptive law (denoted as UA) are displayed in Table II. We can observe that the proposed TS-FTC scheme provides better lateral stability and STT than UA in faulty case, which evidences that the parameter update is able to improve the FTC performance against faults.

V. CONCLUSION

A triple-step fault-tolerant control scheme was proposed to realize the motion control of IWM EGVs under inaccurate parameters, external disturbances, three types of actuator faults and a driver in the loop. This scheme was established based on the triple-step methodology, which employed adaptive and Lyapunov techniques to eliminate its dependence on parameter uncertainties and faults. It is a high confidence method in the sense that the robustly asymptotic tracking performance holds in vehicle, and a driving signal is provided and used for driver guiding and evaluating. Numerical simulations using a

high-fidelity veDYNA and full-vehicle model were carried out to verify the effectiveness of the developed control.

We would like to point out, in this paper, that we studied the cases of loss-of-effectiveness, additional and stuck faults inside the in-wheel motors and active steering systems. However, the cases that some actuators completely lose the control power are not involved, typically as the steering system is in a total failure. Moreover, the research on the perception behavior and the uncertainty in the human drivers as well as the extreme driving FTC under faults are still open issues. The last should be investigated by the experimental validation of the proposed control method through a real vehicle, and improve the control performance during implementation.

REFERENCES

- [1] F. Riaz and M. A. Niazi, "Road collisions avoidance using vehicular cyber-physical systems: A taxonomy and review," *Complex Adaptive Syst. Model.*, vol. 4, no. 15, pp. 1–34, 2016.
- [2] R. N. Jazar, *Vehicle Dynamics: Theory and Application*. New York, NY, USA: Springer-Verlag, 2008.
- [3] J. Wang and R. G. Longoria, "Coordinated and reconfigurable vehicle dynamics control," *IEEE Trans. Control Syst. Technol.*, vol. 17, no. 3, pp. 723–732, May 2009.
- [4] F. Wu, T. J. Yeh, and C. Huang, "Motor control and torque coordination of an electric vehicle actuated by two in-wheel motors," *Mechatronics*, vol. 23, no. 1, pp. 46–60, 2013.
- [5] F. Baronti, A. Lazzeri, R. Roncella, R. Saletti, and S. Saponara, "Design and characterization of a robotized gearbox system based on voice coil actuators for a formula SAE race car," *IEEE-ASME Trans. Mechatronics*, vol. 18, no. 1, pp. 53–61, Feb. 2013.
- [6] D. Saifia, M. Chadli, H. R. Karimi, and S. Labiod, "Fuzzy control for electric power steering system with assist motor current input constraints," *J. Franklin Inst. B*, vol. 35, no. 2, pp. 562–576, 2015.
- [7] H. Zhang and J. Wang, "Adaptive sliding-mode observer design for a selective catalytic reduction system of ground-vehicle diesel engines," *IEEE-ASME Trans. Mech.*, vol. 21, no. 4, pp. 2027–2038, Aug. 2016.
- [8] C. Houben and S. Houben, "Endowing advanced driver assistance systems with fault tolerance," *Annu. Rev. Control*, vol. 39, pp. 58–67, 2015.
- [9] J. Nilsson, M. Brannstrom, J. Fredriksson, and E. Coelingh, "Longitudinal and lateral control for automated yielding maneuver," *IEEE Trans. Intell. Transp. Syst.*, vol. 17, no. 5, pp. 1404–1414, May 2016.
- [10] F. Y. Wang, "Parallel control and management for intelligent transportation systems: Concepts, architectures and applications," *IEEE Trans. Intell. Transp. Syst.*, vol. 11, no. 3, pp. 630–638, Sep. 2010.
- [11] R. Wang, H. Zhang, and J. Wang, "Linear parameter-varying controller design for four wheel independently-actuated electric ground vehicles with active steering systems," *IEEE Trans. Control Syst. Technol.*, vol. 22, no. 4, pp. 1281–1296, Jul. 2014.
- [12] H. Zhang and J. Wang, " H_∞ observer design for LPV systems with uncertain measurements on scheduling variables: Application to an electric ground vehicle," *IEEE-ASME Trans. Mechatronics*, vol. 21, no. 3, pp. 1659–1670, Jun. 2016.
- [13] S. X. Ding, *Model-Based Fault Diagnosis Techniques Design Schemes Algorithms and Tools, Second Ed.* Berlin, Germany: Springer-Verlag, 2013.
- [14] R. J. Patton, *Fault-Tolerant Control*. London, U.K.: Springer, 2015.
- [15] S. Yin, B. Xiao, S. X. Ding, and D. Zhou, "A review on recent development of spacecraft attitude fault-tolerant control system," *IEEE Trans. Ind. Electron.*, vol. 63, no. 5, pp. 3311–3320, May 2016.
- [16] M. A. Khanesar, O. Kaynak, and H. Gao, "Direct model reference adaptive fuzzy control of network SISO nonlinear systems," *IEEE-ASME Trans. Mechatronics*, vol. 21, no. 1, pp. 205–213, Feb. 2016.
- [17] R. Wang, H. Jing, C. Hu, M. Chadli, and F. Yan, "Robust H_∞ output-feedback yaw control for in-wheel motor driven electric vehicles with differential steering," *Neurocomputing*, vol. 173, pp. 676–684, 2016.
- [18] R. Wang and J. Wang, "Fault-tolerant control with active fault diagnosis for four-wheel independently driven electric ground vehicle," *IEEE Trans. Veh. Technol.*, vol. 60, no. 9, pp. 4276–4287, Nov. 2011.
- [19] M. Plochl and J. Edelmann, "Driver models in automobile dynamics application," *Veh. Syst. Dyn.*, vol. 45, no. 7/8, pp. 699–741, 2007.

- [20] X. Na and D. J. Cole, "Linear quadratic game and non-cooperative predictive methods for potential application to modelling driver-AFS interactive steering control," *Veh. Syst. Dyn.*, vol. 51, no. 2, pp. 165–198, 2013.
- [21] S. L. Jamson, D. L. Hibberd, and A. H. Jamson, "Drivers' ability to learn eco-driving skills; effects on fuel efficient and safe driving behavior," *Transp. Res. Part C*, vol. 58, pp. 657–668, 2015.
- [22] P. Raksincharoensak, T. Mizushima, and M. Nagai, "Direct yaw moment control system based on driver behaviour recognition," *Veh. Syst. Dyn.*, vol. 46, pp. 911–921, 2008.
- [23] Y. Dong, Z. Hu, K. Uchimura, and N. Murayama, "Driver inattention monitoring system for intelligent vehicles: A review," *IEEE Trans. Intell. Transp. Syst.*, vol. 12, no. 2, pp. 596–614, Jun. 2010.
- [24] H. Chen, X. Gong, Q. Liu, and Y. Hu, "A triple-step method to design nonlinear controller for rail pressure of GDI engines," *IET Control Theory Appl.*, vol. 8, no. 11, pp. 948–959, 2014.
- [25] J. Guo, P. Hu, and R. Wang, "Nonlinear coordinated steering and braking control of vision-based autonomous vehicles in emergency obstacle avoidance," *IEEE Trans. Intell. Transp. Syst.*, vol. 17, no. 11, pp. 3230–3240, Nov. 2016.
- [26] F. Wang, H. Chen, and D. Cao, "Nonlinear coordinated motion control of road vehicles after a tire blowout," *IEEE Trans. Control Syst. Technol.*, vol. 24, no. 3, pp. 956–970, May 2016.
- [27] S. Mammar, "Two-degree-of-freedom H_∞ optimization and scheduling for robust vehicle lateral control," *Veh. Syst. Dyn.*, vol. 34, no. 6, pp. 401–422, 2000.
- [28] A. Nenine-Neto, S. Scalzi, M. Netto, S. Mammar, and W. Pasillas-Lepine, "Vehicle yaw rate control based on piecewise affine regions," in *Proc. IEEE Intell. Veh. Symp.*, San Diego, CA, USA, Jun. 2010, pp. 21–24.
- [29] T. Qu, H. Chen, D. Cao, H. Guo, and B. Gao, "Switching-based stochastic model predictive control approach for modeling driver steering skill," *IEEE Trans. Intell. Transp. Syst.*, vol. 16, no. 1, pp. 365–375, Feb. 2015.
- [30] A. J. Pick and D. J. Cole, "Neuromuscular dynamics in the driver-vehicle system," *Veh. Syst. Dyn.*, vol. 44, pp. 624–631, 2006.
- [31] N. Rhodes and K. Pivik, "Age and gender differences in risky driving: The roles of positive affect and risk perception," *Accident Anal. Prevention*, vol. 43, no. 3, pp. 923–931, 2011.
- [32] D. Lu and K. Guo, "Unitire steady state model: Overview and application," in *Proc. IEEE 3rd Int. Conf. Adv. Comput. Control*, Harbin, China, Jan. 2011, pp. 341–345.



Yulei Wang received the B.S. degree in theoretical physics from Nankai University, Tianjin, China, in 2008, and the Ph.D. degree in control science and engineering from Harbin Institute of Technology, Harbin, China, in 2013. From 2010 to 2012, he was a joint Ph.D. student with the Institute for Automatic Control and Complex Systems, University of Duisburg-Essen, Duisburg, Germany.

Since 2013, he has been a member of the Department of Control Science and Engineering, Jilin University, Changchun, China. His current research interests include fault detection and isolation, fault-tolerant control, and applications in mechatronic systems.



Shuyou Yu received the B.S. and M.S. degrees in control science and engineering from Jilin University, Changchun, China, in 1997 and 2005, respectively, and the Ph.D. degree in engineering cybernetics with the University of Stuttgart, Stuttgart, Germany, in 2011.

From 2010 to 2011, he was a research and teaching assistant, with the Institute for Systems Theory and Automatic Control, the University of Stuttgart, Germany. In 2012, he is currently an Associate Professor at the Department of Control Science and Engineering, Jilin University, Changchun, China. His research interests include model predictive control, robust control, and applications in mechatronic systems.



Jingxin Yuan received the B.S. degree in control science and engineering from Jilin University, Changchun, China, in 2016. Since 2016, she has been a M.S. student with the Institute of Control Science and Engineering, Jilin University, China.

Her current research interests include fault detection and isolation, fault-tolerant control, and applications in mechatronic systems.



Hong Chen (M'02–SM'12) received the B.S. and M.S. degrees in process control from Zhejiang University, Hangzhou, China, in 1983 and 1986, respectively, and the Ph.D. degree in engineering cybernetics from the University of Stuttgart, Stuttgart, Germany, in 1997.

In 1986, she joined Jilin University of Technology, China. From 1993 to 1997, she was a Wissenschaftlicher Mitarbeiter with the Institut fuer Systemdynamik und Regelungstechnik, University of Stuttgart, Germany. Since 1999, she has been a Professor with Jilin University, where she is currently a Tang Aoqing Professor. Her current research interests include triple-step nonlinear control, model predictive control, optimal and robust control, and applications in process engineering and mechatronic systems.